Article

Green-, Red-, and NIR-Emitting Polymer Dot Probes for Simultaneous Multicolor Cell Imaging with a Single Excitation Wavelength

Ji-Eun Jeong, Mohammad Afsar Uddin, Hwa Sook Ryu, Hee-Chang Kim, Minsu Kang, Joonyoung Francis Joung, Sungnam Park, Sang-Hee Shim, and Han Young Woo

Chem. Mater., **Just Accepted Manuscript** • DOI: 10.1021/acs.chemmater.0c02172 • Publication Date (Web): 05 Jul 2020

Just Accepted

is published by the American Chemical Society. 1155 Sixteenth Street N.W., Washington, DC 20036

Green-, Red-, and NIR-Emitting Polymer Dot Probes for Simultaneous Multicolor Cell Imaging with a Single Excitation Wavelength

Ji-Eun Jeong,[†] Mohammad Afsar Uddin,[‡] Hwa Sook Ryu,[†] Hee-Chang Kim,[†,§] Minsu Kang,[†,§] Joonyoung Francis Joung,[†] Sungnam Park,[†] Sang-Hee Shim,[†,§,] and Han Young Woo[†,*]*

[†]Department of Chemistry, Korea University, Seoul 136-713, Republic of Korea.

[‡] Instituto de Ciencia de Materiales de Madrid, Madrid, 20849, Spain.

[§] Center for Molecular Spectroscopy and Dynamics, Institute for Basic Science (IBS), Korea University, Seoul, 02841, Republic of Korea.

*E-mail: hywoo@korea.ac.kr (H. Y. Woo), sangheeshim@korea.ac.kr (S.-H. Shim)

Abstract

We report newly synthesized fluorescence resonance energy transfer (FRET)-based green-, red-, and near-infrared (NIR)-emitting polymer dot (Pdot) probes. Fluorescent Pdots (~60 nm) were prepared with a green-emissive conjugated polymer (PPDT-P, donor) alone or mixing the donor with a red or NIR-emitting fluorophore (T-DCS or ITIC, acceptor), where an optically inert matrix polymer (PSMA) was mixed together to minimize the aggregation-caused quenching by diluting the fluorophores and surface functionalization for further bioconjugation with antibodies for active targeting. Highly fluorescent green-emissive PPDT-P Pdots were prepared with a photoluminescence (PL) quantum efficiency of ~30% and the FRET-mediated red and NIR PL was intensified by 5.3 to 8.5 times (with high FRET ratios of ~9) via the efficient energy transfer (FRET efficiency of 80-98%) and antenna effect, compared with the signals obtained via direct excitation of the fluorophores in Pdots. All three types of Pdot/antibody conjugates were simultaneously immunostained to COS-7 cells (showing minimal cross-reactivity), reducing the tedious sequential immunostaining process to a single step. Finally, we obtained high-contrast three-color cell images with little spectral leakthrough by exciting all the probes simultaneously at a single wavelength at 405 nm without the need for a complicated or expensive multiple-excitation setup.

1. INTRODUCTION

π-Conjugated semiconducting polymers (CPs) have useful optical and electrical properties and great potential for utilization in optoelectronic devices, chemo-/biosensors, and biological imaging.[1-4] In particular, the intrinsic light harvesting and molecular wire effect of CPs, as well as the large absorption cross sections, render them applicable as optical platforms in fluorescent chemo- and bioassays with high sensitivity.[5] To utilize hydrophobic CPs with poor water-solubility as optical probes in aqueous biological specimens, CPs are often coprecipitated with an amphiphilic matrix to produce polymer dots (Pdots).[6-9] Pdots have many advantages, such as easy preparation, high brightness, large absorption, surface functionalization, excellent photostability, good water stability, and biocompatibility; therefore, they have been studied as fluorescent probes with molecular specificity to investigate biomolecular interactions and to visualize subcellular structures and processes.[10-14]

Applications based on multicolor fluorescence imaging have exhibited a remarkable growth in basic science and clinical diagnostics.[15, 16] To compose a multicolor image, different biomolecular species are labeled with different fluorophores[17]; this renders it necessary to employ different excitation sources for each fluorophore, which in turn increases the instrument cost and measurement complexity. Rong et. al. synthesized a series of BODIPY-containing copolymers by coupling the donor (fluorene, benzothiadiazole, or 4,7-bisthienyl-2,1,3-benzothiadiazole) and acceptor (BODIPY derivatives) moieties to modulate the intramolecular energy transfer for multicolor fluorescence imaging.[14] In this report, green-emissive 520 Pdots were excited at 405 nm, while red-emissive 600 Pdots and deep red-emissive 690 Pdots were excited at 488 nm for multicolor imaging. Because 520 Pdots and 600/690 Pdots have the complementary absorptions in a range of 300-500 nm, these Pdots cannot be excited at a same wavelength. Spectrally similar fluorophores can be excited with a single excitation source and

distinguished using spectral detection and linear unmixing. However, the detection system is expensive, and the resultant image can suffer from a spectral leakthrough. Therefore, it is desired to have a set of fluorophores with similar absorption spectra and distinguishable emission spectra to obtain crosstalk-free and high-contrast multicolor imaging with a single excitation source and standard filter sets. Few researchers have attempted multicolor imaging with single wavelength excitation. Xing and Wu reported water-soluble carbon dots, the size of which was controlled by modulating cutting temperatures, showing excitation-independent emission.[18] They realized multicolor emission in the range of blue to yellow, upon excitation at 360 nm. Liu et al. tuned the emission color of aggregation-induced emission (AIE) molecules based on tetraphenylethylene (TPE) by controlling the degrees of intramolecular charge transfer through the introduction of different electron-donating and electron-accepting moieties to TPE.[19] Two types of AIE-based structures exhibited a large difference in the emission spectra but a small difference in the absorption spectra. Despite their successful emission at different wavelengths upon a single irradiation, challenges such as the unavoidable spectral overlap, lack of surface modification, and limited number of targeting organelles prohibit the structures from becoming practical multicolor probes.

Fluorescence resonance energy transfer (FRET) can be utilized for multicolor imaging because a single donor excitation can result in fluorescence emission of various acceptor dyes. FRET involves non-radiative energy transfer between donor and acceptor molecules via dipole–dipole coupling and has been widely used for fluorescent and ratiometric sensing.[20-22] Because the FRET efficiency is inversely proportional to the donor–acceptor intermolecular distance raised to the sixth power, Pdots that encage the fluorophores within the nano-sized particles can be an appropriate platform to locate donor and acceptor dyes in close proximity. Furthermore, the photoluminescence (PL) of red- and near-infrared (NIR)-emitting probes can be enhanced

via the antenna effect of CPs, which can be advantageous for biological imaging owing to the deep tissue penetration and negligible autofluorescence.

In this study, green, red, NIR-emissive three types of FRET-based Pdot probes were prepared with different target specificity for multicolor biological imaging (**Scheme 1**). We successfully demonstrated a multicolor fluorescence imaging with semiconducting Pdots by single wavelength excitation, which is the first report to the best of our knowledge. By precipitating the green-emitting conjugated polymer, poly[(2,5-bis(2-hexyldecanoate)phenylene)-alt-(5,5'-(1,4-phenylene)-bis(thiophen-2-yl))] (PPDT-P) alone or by co-precipitating PPDT-P (as a FRET donor) with the red-emitting fluorophore, (2E,2'E)-3,3'-(2,5-bis((2-hexyldecyl)oxy)-1,4-phenylene)-bis(2-([2,2'-bithiophen]-5-yl)acrylonitrile) (T-DCS) or the NIR-emitting fluorophore, 3,9-bis(2-methylene-(3-(1,1-dicyanomethylene)-indanone))-5,5,11,11-tetrakis(4-hexylphenyl)-dithieno[2,3-d:2',3'-d']-s-indaceno[1,2-b:5,6-b']dithiophene (ITIC) (as a FRET acceptor), we prepared green-, red-, and NIR-emitting Pdots. A FRET donor (PPDT-P) showed a suppressed aggregation-caused quenching (ACQ) in Pdots, showing a PL quantum yield (PLQY) of ~30% even in a condensed solid state. Because all the Pdots had PPDT-P as a main component, the three Pdots had maximum absorption at the same wavelength (determined by PPDT-P) and could be excited using a single excitation wavelength. The FRET-mediated red and NIR emissions were significantly enhanced (by factors of 5.3 and 8.5, respectively) compared with the signals obtained via direct excitation of red and NIR fluorophore in Pdots. A remarkably high FRET efficiency (80-98%) in red- and NIR-emitting Pdots and the FRET-mediated emissions with high color purity were obtained. The surface of each Pdot was functionalized with three types of secondary antibodies for specific targeting into different subcellular regions. By co-staining COS-7 cells with all three Pdot probes simultaneously,

multi-color images of tubulin, vimentin, and mitochondria were successfully obtained by exciting all the probes at a single wavelength.

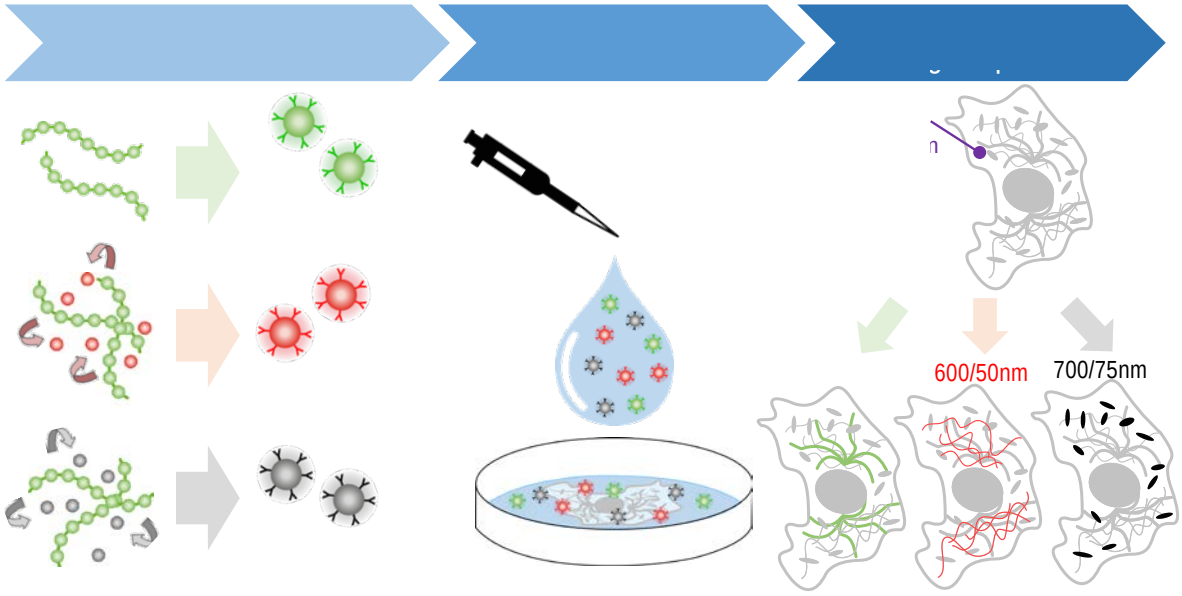

Scheme 1. Schematic for multicolor subcellular imaging with single wavelength excitation.

2. RESULTS AND DISCUSSION

2.1. Material Synthesis and Characterization

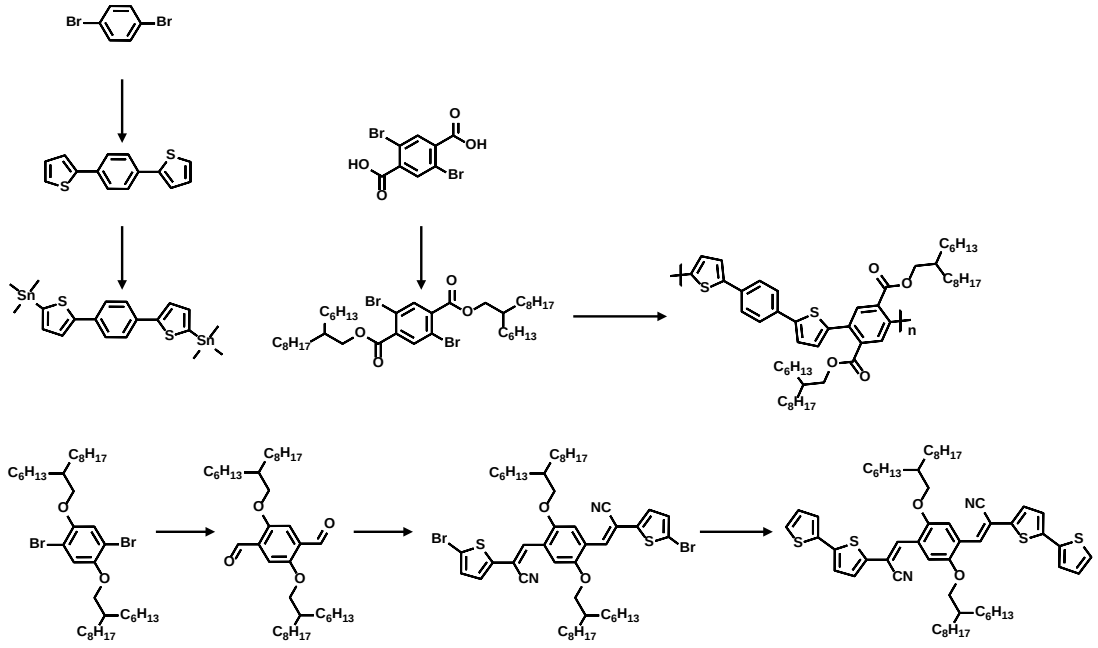

Scheme 2. Synthesis routes for PPDT-P and T-DCS. i) 2-(tributylstannyl)thiophene, $Pd(PPh_3)_4$, THF; ii) *n*-BuLi, Me_3SnCl; iii) $SOCl_2$, pyridine, $C_{16}H_{33}OH$, DCM; iv) $Pd_2(dba)_3$, tris(*o*-tolyl)phosphine, toluene; v) THF, *n*-BuLi, DMF, –78 ℃; vi) 2-(5-bromothiophen-2-yl)acetonitrile, *t*-BuOK, *t*-BuOH, 50 ℃.; vii) 2-(tributylstannyl)thiophene, $Pd_2(dba)_3$, tris(*o*-tolyl)phosphine, toluene.

A green-emissive conjugated polymer PPDT-P and a red-emissive fluorophore T-DCS were newly synthesized, as shown in **Scheme 2**. A NIR-emissive conjugated molecule ITIC was purchased from Solarmer (China). The synthesis procedures are described in the Supporting Information. In accordance with a previously reported procedure,[23] 1,4-dibromobenzene (1) was reacted with 2-(tributylstannyl)thiophene to produce 1,4-bis(thiophen-2-yl)benzene (2) with a 79% yield, and subsequent stannylation yielded 1,4-bis(5-(trimethylstannyl)thiophen-2-yl)benzene (M1) with a 75% yield. 1,4-Dibromo-2,5-bis(2-hexyldecanoate)benzene (M2) was

prepared via the esterification reaction of 2,5-dibromoterephthalic acid (3) and 2-hexyl-1-decanol together with a catalytic amount of pyridine in dichloromethane (DCM). The green-emissive polymer PPDT-P was synthesized via Stille coupling of M1 and M2 in toluene with tris(dibenzylideneacetone)dipalladium (0) ($Pd_2(dba)_3$) and tri(*o*-tolyl)phosphine as a catalytic system (78% yield, number-average molecular weight of M_n = 22,600 Da). After formylation of 1,4-dibromo-2,5-bis(2-decyltetradecyloxy)benzene (4), compound 5 was reacted with 2-(5-bromothiophen-2-yl)acetonitrile in the presence of *t*-BuOK in *t*-BuOH to obtain (2E,2'E)-3,3'-(2,5-bis((2-hexyldecyl)oxy)-1,4-phenylene)-bis(2-(5-bromothiophen-2-yl)acrylonitrile (6).[24] The red-emissive T-DCS was prepared with a 72% yield via Stille coupling between compound 6 and 2-(tributylstannyl)thiophene in toluene.

2.2. Preparation and optimization of FRET-based multicolor Pdots

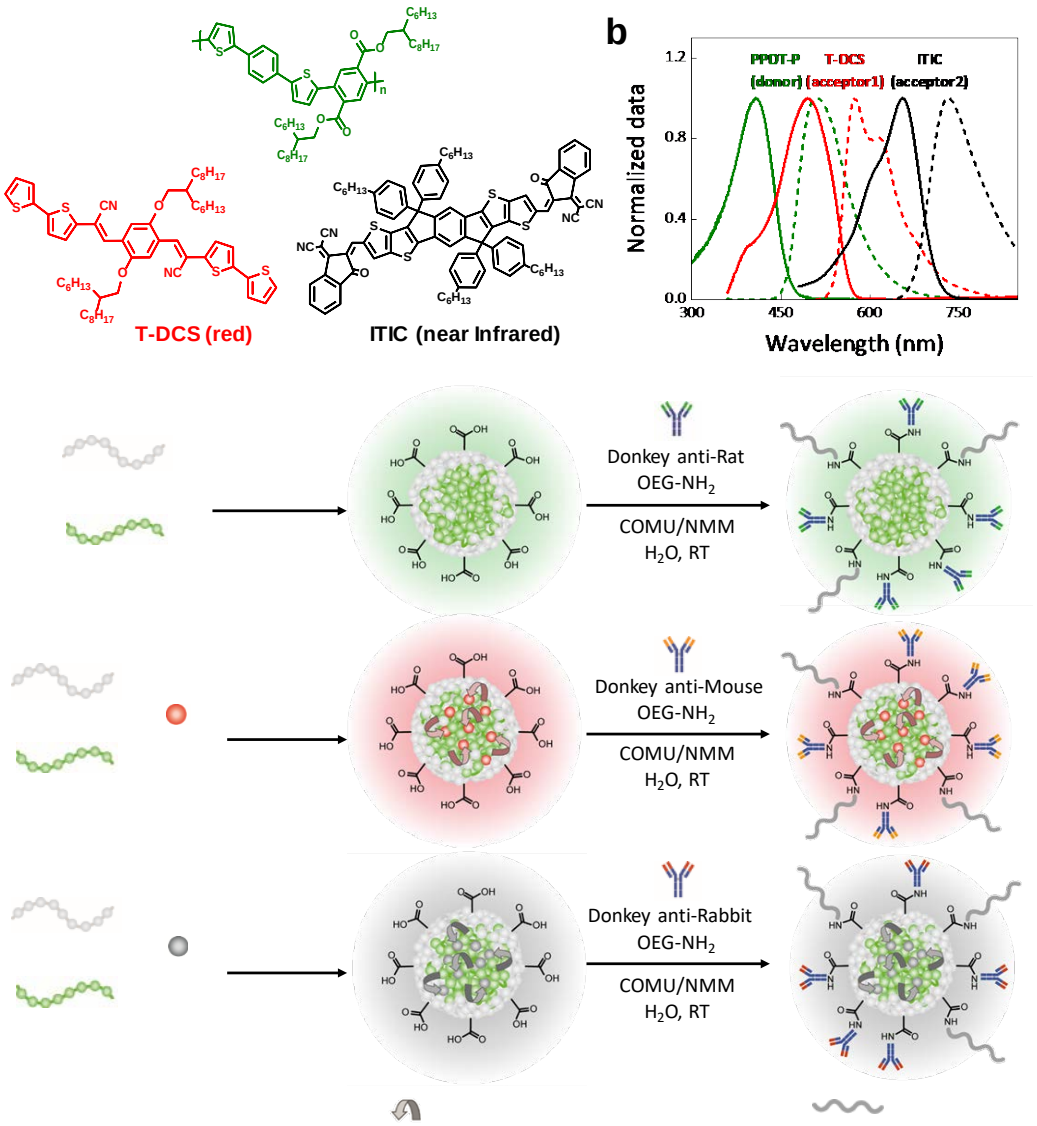

Figure 1. (a) Chemical structures of FRET donor (PPDT-P), acceptor1 (T-DCS), and acceptor2 (ITIC). (b) Absorption (solid) and emission (dashed) spectra of PPDT-P, T-DCS, and ITIC in THF. (c) Schematic of preparation of green-, red-, and NIR-emitting Pdots and surface modification with different antibodies.

To prepare the FRET-based multicolor-emissive Pdots, the FRET donor (PPDT-P) and acceptors (T-DCS or ITIC) were designed and selected by considering their bandgap and

spectral overlap between the donor emission and acceptor absorption (**Figure 1**). In tetrahydrofuran (THF), the maximum absorption and PL wavelengths of PPDT-P were observed at λ_{abs} = ~410 nm and λ_{PL} = ~510 nm, respectively, with a PLQY of ~43%, relative to a freshly prepared fluorescein solution in water at pH=11. As shown in Figure 1b, the absorption spectra of the red-emitting T-DCS and NIR-emitting ITIC had peaks at λ_{abs} = 495 nm and 655 nm, respectively, exhibiting significant spectral overlap with the emission of PPDT-P. The maximum PL emission in THF was measured at λ_{PL} = 575 nm (PLQY = ~17%) for T-DCS and at λ_{PL} = 732 nm (PLQY = ~3%) for ITIC, allowing the facile tuning of the PL emission ranges (green to red and NIR) via FRET with a single excitation wavelength.

To examine the optical properties of the three fluorophores in a condensed aggregated phase, Pdots were first prepared with a single fluorophore. PPDT-P, T-DCS, or ITIC was dissolved in THF together with poly(styrene-co-maleic anhydride) (PSMA, M_n ~1600 Da, ~1.3:1 mole ratio of styrene:maleic anhydride) as a matrix, followed by a quick transfer to an aqueous solution under vigorous sonication, precipitating nano-sized Pdots.[25, 26] The PSMA matrix played several important roles to control the local environment around the fluorophores and particle surface.[27] i) By encaging both the FRET donor and acceptor inside the PSMA matrix, they were kept in close proximity to induce efficient energy transfer. ii) PSMA prevented excessive self-aggregation of emitting species by diluting the photoactive fluorophore concentration in the photo-inactive matrix, reducing the ACQ. iii) In the formation of Pdots, the maleic anhydride units in the PSMA were hydrolyzed to carboxylic acid groups, leading to further surface functionalization for molecular-specific targeting. To identify the optimum concentration of PSMA within the Pdots, the precursor solutions of PPDT-P/PSMA, T-DCS/PSMA, and ITIC/PSMA in THF with various mixing ratios ([PSMA] = 0.02–0.09 mg/mL, [precursor] = [PSMA] + [PPDT-P, T-DCS, or ITIC] = 0.1 mg/mL) were precipitated into water, providing a

series of Pdots with different [PSMA]:[fluorophore] ratios. With the increasing [PSMA], the PLQY of the resulting Pdots increased, indicating the need for excess PSMA to minimize the self-quenching effect. Finally, the optimum [PSMA] for maximum PL emission was determined to be 0.08 mg/mL.

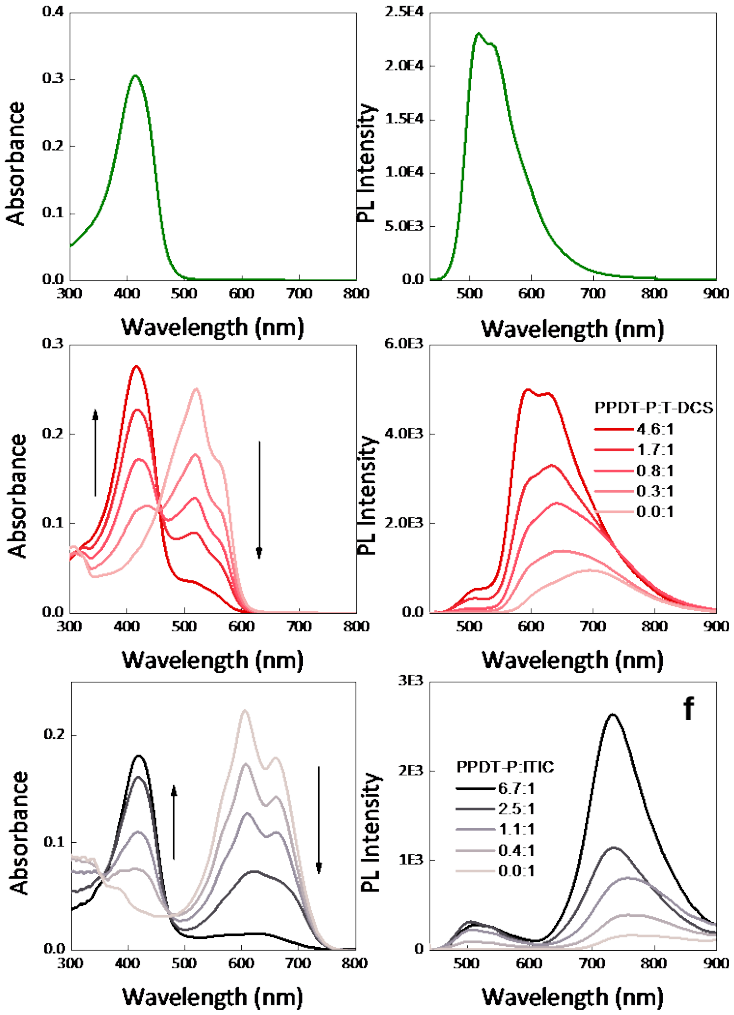

Figure 2. (a, c, e) UV–vis and (b, d, f) PL spectra of PPDT-P/PSMA (a, b), PPDT-P/T-DCS/PSMA (c, d), and PPDT-P/ITIC/PSMA (e, f) Pdots in an aqueous solution with different D:A molar ratios. The PL spectra were obtained by exciting the donor polymer (PPDT-P) at 420 nm.

Compared with the PPDT-P solution in THF, slightly red-shifted absorption and PL maxima for the PPDT-P Pdots were observed (at 420 and 515 nm, respectively), indicating agglomerated PPDT-P molecules (**Figure 2**a and b). In the aggregated phase, T-DCS and ITIC also exhibited red-shifted PL spectra, with λ_{PL} = 695 and 778 nm, respectively (Figure S1). Intermolecular aggregation of conjugated polymer chains within a Pdot matrix often results in a significant PL quenching, which should be carefully considered in the design of Pdot-based fluorescent probes. Interestingly, the PLQY of ~43% was measured for PPDT-P in solution (THF) and the PPDT-P aggregates in Pdots still maintained a high PLQY of ~30% in a condensed solid state, indicating that the ACQ is not significant. As shown in Table S1, the PLQY of PPDT-P/PSMA Pdots was significantly higher or comparable relative to those of other reported Pdots by careful polymer design to suppress the ACQ. To prevent a serious aggregation of polymers, we introduced a tilted polymer backbone consisting of repetitive phenylene and thiophene units as well as branched side-chains.[28-30] Because torsional angles along the main chain have a great effect on the intermolecular packing and PL quenching, the polymer chain conformation was modulated to optimize the π-conjugation and exciton migration with minimized ACQ. The incorporation of the phenylene moieties in a polymer backbone breaks the chain planarity of polythiophenes and avoids a serious intermolecular packing.[31, 32] The energy-minimum conformational analysis of PPDT-P was performed by density functional theory (DFT) calculation (basis set: B3LYP/6-31g(d,p)) (Figure S2). By introducing the phenylene units in a polymer backbone, torsional angles between thiophene and phenylene (Φ_1, Φ_2, Φ_5, and Φ_6) moieties were calculated to be ~24°, leading to a twisted backbone. In addition, the steric hindrance by incorporating 2-hexyldecanoate side-chains onto a phenylene ring further increases a torsional angle (Φ_3, Φ_4, and Φ_7 = ~51°). Thus, PPDT-P which forms a randomly aggregated structure (amorphous) with suppressed ACQ is a promising

candidate as an efficient FRET donor to improve the energy transfer even in the highly aggregated state.

Then, a multicolor set of green-, red-, and NIR-emitting Pdots was prepared by precipitating the green-emissive PPDT-P (FRET donor) alone or by co-precipitating the mixture of PPDT-P and red or NIR-emitting fluorophores (FRET acceptor) together with PSMA as a matrix. Ideal FRET-based multicolor fluorescent probes require bright FRET-induced PL for a high signal-to-noise ratio as well as a high FRET ratio ($I_{acceptor}/I_{donor}$, where $I_{acceptor}$ represents the PL intensity at the λ_{PL} of the acceptor and I_{donor} represents the PL intensity at the λ_{PL} of the donor) for color purity. To satisfy the requirements, the FRET system in the red- and NIR-emitting Pdots was optimized by controlling the mixing ratio of the FRET donor and acceptor. Donor and acceptor stock solutions (1 mg/mL) in THF were mixed at various molar ratios of [donor]/[acceptor]: 0–4.6 and 0–6.7 for T-DCS- and ITIC-based FRET Pdots, respectively. As a Pdot matrix, PSMA (0.08 mg/mL) was also introduced. Finally, the precursor solutions with different mixing ratios (total concentration of 0.1 mg/mL) were quickly transferred to an aqueous solution under vigorous sonication. As the donor-to-acceptor molar ratio within the Pdots increased, the absorption of the FRET donor (PPDT-P) at ~420 nm increased, and the acceptor absorption at ~520 nm for T-DCS or ~620 nm for ITIC decreased gradually (Figure 2c and e).

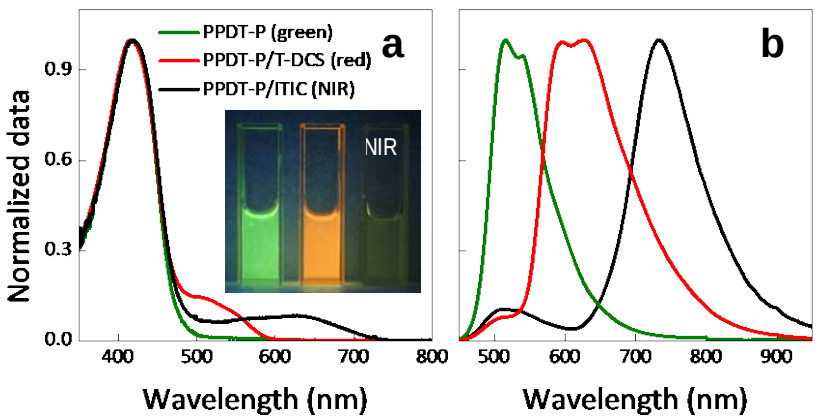

Figure 3. Normalized (a) UV–vis and (b) PL spectra of PPDT-P/PSMA, PPDT-P/T-DCS/PSMA and PPDT-P/ITIC/PSMA Pdots in aqueous solution. PL spectra were obtained by exciting at 420 nm. Inset in (a) shows the photograph of green (left), red (middle) and NIR (right)-emissive Pdots under illumination with a handheld UV lamp at 365 nm.

In the presence of PPDT-P, the energy transfer within the PPDT-P/T-DCS/PSMA and PPDT-P/ITIC/PSMA Pdots was evident from the loss of donor emission and the significant increase in the acceptor emission upon the excitation of PPDT-P at 420 nm (Figure 2d and f). With increasing of [PPDT-P], the FRET-induced acceptor PL enhanced via the efficient energy transfer with gradually blue-shifted emissions, indicating the reduced self-aggregation of the acceptors. Additionally, the FRET ratio was improved by modulating the donor-to-acceptor ratio. Finally, the optimum D:A molar ratio that yielded the highest FRET-induced PL intensity as well as the largest FRET ratio was determined to be 4.6:1 for PPDT-P/T-DCS and 6.7:1 for PPDT-P/ITIC (**Figure 3**). In Figure S3, the strong absorption (absorbance ~0.27) at ~420 nm originates from PPDT-P and the small peaks at ~520 and ~620 nm (absorbance ~0.03 and ~0.02) are assigned to absorptions from T-DCS and ITIC, respectively. Due to the presence of excess PPDT-P in red- and NIR-Pdots, the strong light absorption by PPDT-P and following FRET to the acceptors (T-DCS and ITIC) can occur to yield the intensified FRET-mediated PL by exciting donor polymer (PPDT-P) at 405 nm, which is known as signal amplification via the antenna effect.[5, 33, 34] The FRET-mediated red and NIR emissions were significantly enhanced (by factors of 5.3 and 8.5, respectively) compared with the signals obtained via direct excitation of red and NIR fluorophores in Pdots at 520 and 620 nm, respectively. With the optimum blending ratio, high FRET ratios of ~9 were measured for both the PPDT-P/T-DCS/PSMA and PPDT-P/ITIC/PSMA Pdots. By further increasing the D:A mixing ratio, the FRET-induced PL

emission was saturated or reduced with a concomitant increase in the PPDT-P emission, decreasing the FRET ratio (Figure S4).

To determine the quenching efficiency of PPDT-P by each acceptor (T-DCS or ITIC), the Stern−Volmer plots (Figure S5) were prepared by measuring PL quenching with varying the quencher concentration.[35-37] The obtained results show that each single T-DCS and ITIC molecule can quench ~56 and ~79 polymer repeating units (RU), respectively, indicating highly efficient energy transfer from PPDT-P to acceptors. It is worthy to mention that efficient exciton migration along the conjugated polymer backbone is an important factor to yield the large K_{sv} values. Similar results have been reported by Zhou et. al. to show ~60 times greater K_{sv} for conjugated polymers compared to that of small molecular fluorophores.[5] Additionally, the FRET efficiencies in the Pdots were estimated by measuring the PL decays of the donor (PPDT-P) in the presence and absence of the acceptors (T-DCS and ITIC) via the time-correlated single photon counting (TCSPC) method as shown in Figure S6. The amplitude-weighted average PL lifetime of PPDT-P without acceptors was determined to be 0.547 ns. In the presence of acceptors, the PL decays of PPDT-P were fitted using the modified FRET model (for the FRET system with randomly dispersed donors and acceptors) reported by Fung et. al.[38] The FRET efficiencies of PPDT-P/T-DCS/PSMA (D:A = 4.6:1) and PPDT-P/ITIC/PSMA (D:A = 6.7:1) Pdots in aqueous solution were determined to be 80% and 98%, respectively. The high FRET efficiencies show a good agreement with the measured K_{sv}, indicating efficient energy transfer from PPDT-P to the acceptors.

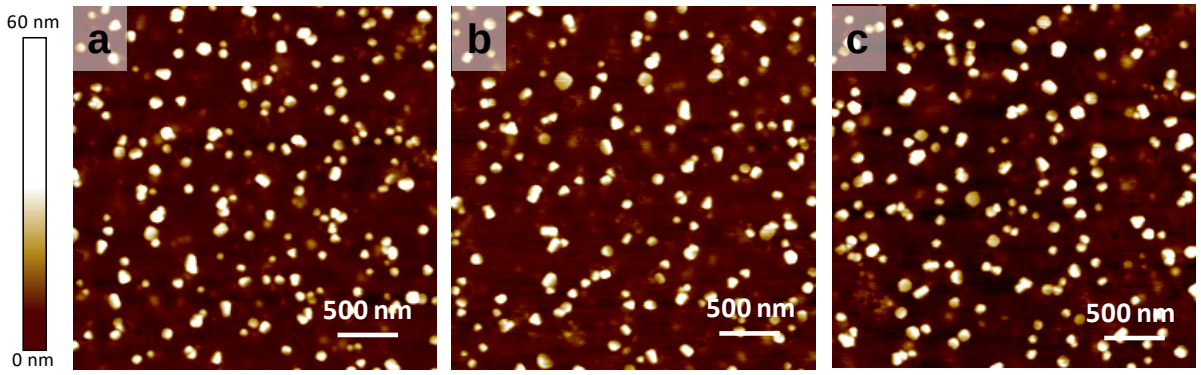

Figure 4. AFM images of (a) PPDT-P/PSMA, (b) PPDT-P/T-DCS/PSMA, and (c) PPDT-P/ITIC/PSMA Pdots.

The size and shape of nanoparticles may play an important role in cellular uptake. To determine the hydrodynamic diameter, dynamic light scattering (DLS) measurements of Pdots in an aqueous solution were performed using a 633 nm laser source (Figure S7). The average diameter of the green-, red-, and NIR-emissive Pdots was ~60 nm according to the constrained regularization method for inverting data (CONTIN) analysis.[39] As shown in Figure S7d, all Pdots show negative zeta potentials, ranging from -37 to -52 mV due to the presence of negatively charged carboxylate groups on the Pdot surfaces.[40, 41] No aggregation or significant changes in the optical properties were observed for the three types of Pdots even after several months, indicating the pronounced stability of the dispersed Pdots in aqueous media. Similar results have been reported to show that colloids with a zeta potential over (+/–) 30 mV have a long-term colloidal stability.[42] The morphology of the Pdots was also characterized using atomic force microscopy (AFM) (**Figure 4**). The AFM samples were prepared by dropping ~20 μL of a diluted Pdot solution (stock solution of Pdots (~2.5 μg/mL) was diluted by a factor of 20) on a mica substrate. All the Pdots exhibited a spherical shape with an average diameter of ~60 nm, which is consistent with the DLS measurements. There were no significant differences in the particle size or shape for the Pdots with different compositions. Additionally, no

aggregation or significant changes in the optical properties for the three types of Pdots were observed, even after several months, indicating the stability of the dispersed Pdots in the aqueous media. In a previous study, nanoparticles with a size of 20–100 nm were reported to easily penetrate the plasma membrane of cells to localize in specific organelles with the aid of a permeabilizing reagent.[43-46] The size of the prepared Pdots is expected to be suitable for further immunostaining.

The photostability of PPDT-P/PSMA Pdot probes (50 μg/mL) in water was measured under continuous illumination of an excitation laser light (405 nm, 100 mW) (Figure S8). For comparison, a fluorescein solution (50 μM) was also prepared in water (pH 11) as a control. The fluorescence intensity of PPDT-P/PSMA Pdots remained ~90% of their initial intensity under continuous irradiation for 300 s, while fluorescein showed a severe intensity decrease within 60 s, suggesting high photostability of the Pdots. The excellent photostability of Pdots compared to single molecule fluorophores can be attributed to the larger number density of emitting units inside Pdots. In addition, encapsulation of luminescent fluorophores with a Pdot matrix also prevents the contact of oxygen (or air), reducing the photooxidation (and/or photobleaching) of fluorophores.[47, 48] We also studied the optical properties of PPDT-P/PSMA Pdots in phosphate buffered saline (PBS, pH 7.4) solutions with changing bovine serum albumin (BSA) concentrations (0-3 wt%). As shown in Figure S9, similar absorption and PL spectra of Pdots were measured in BSA solutions compared to those in water, suggesting their stability in physiological environments. It is expected that the encapsulation with hydrophilic PSMA minimizes the direct contact of hydrophobic fluorophores with aqueous buffering media, prohibiting fluorophores from serious aggregation. Additionally, the emission of PPDT-P/PSMA Pdots in BSA solution was somewhat increased (by ~10%) with compared to that in water. Because the isoelectric point of BSA is 4.8 and it must be negatively charged in PBS.

The surface of Pdots possesses large amounts of carboxylate groups, and the electrostatic repulsion between BSA and Pdots further stabilizes the Pdot dispersion. The optical properties of Pdots remained unchanged in BSA buffered solutions even after 1 week. To evaluate the cytotoxicity of the Pdots, COS-7 cells were incubated with different concentrations of Pdots (0.5-25 μg/mL) in Dulbecco's Modified Eagle Medium (DMEM) buffer, then cellular viability was monitored by optical microscopy. As shown in Figure S10, no obvious morphological change of COS-7 cells was observed in the presence of 10 μg/mL of PPDT-P/PSMA Pdots after incubating for 48 h. Although all the experiments in this study were proceeded with fixed cells, sufficient biocompatibility of the Pdots for live cell imaging was also confirmed.[41, 49, 50] Similar results were also observed in PPDT-P/T-DCS/PSMA and PPDT-P/ITIC/PSMA Pdots.

2.3. Antibody labeling of Pdot surface via COMU coupling

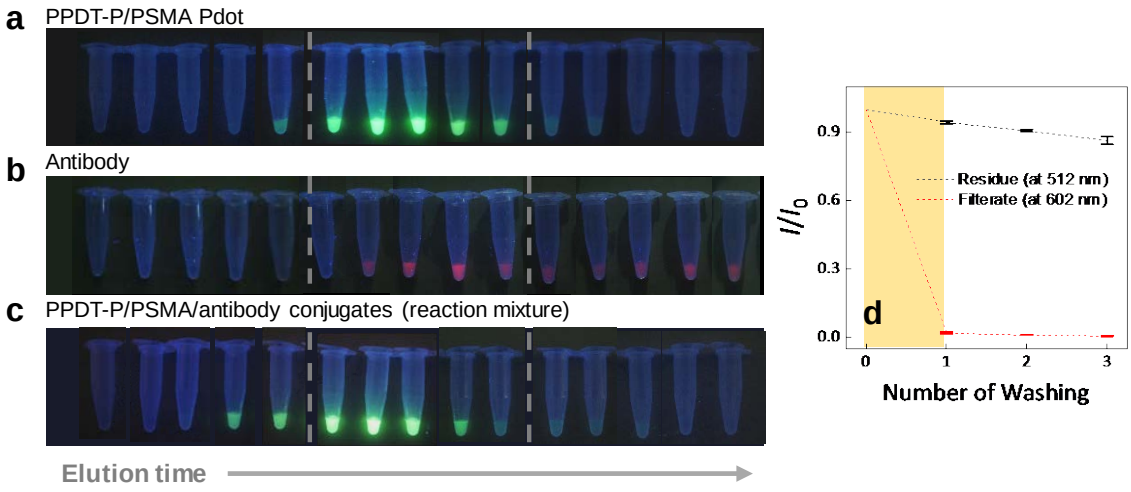

Figure 5. Photographs of separated drops of (a) PPDT-P/PSMA Pdots, (b) secondary antibodies (Donkey anti-Rat), and (c) PPDT-P/PSMA/antibody conjugates depending on the eluting time. Non-fluorescent antibodies were visualized by reacting with Alexa Fluor 568-NHS ester. Irradiation was applied using a handheld UV lamp (365 nm). (d) PL Intensity ratio of PPDT-P/PSMA/antibody conjugates depending on the number of post-washing by centrifugal purification (I/I_0, where I_0 and I are the PL intensities before and after centrifugal filtration at 512 nm for PPDT-P/PSMA/antibody conjugates and 602 nm for excess free antibodies, respectively). The data were obtained from three independent measurements, and the error bars indicate the standard deviation.

During the formation of Pdots, the hydrophobic polystyrene units of the PSMA point toward the inside of the particles, while the hydrophilic maleic anhydride units are exposed on the surfaces. By heating the aqueous solution, the maleic anhydride moieties are hydrolyzed to carboxyl acids, allowing bio-conjugation with antibodies through the formation of amide bonds. To demonstrate specific cellular targeting of three Pdots, three types of amine-functionalized secondary antibodies—Donkey anti-Rat, Donkey anti-Mouse, and Donkey anti-Rabbit—were

coupled with carboxylic acid functional groups on the surface of PPDT-P/PSMA, PPDT-P/T-DCS/PSMA, and PPDT- P/ITIC/PSMA Pdots, respectively (Figure 1c). As a coupling reagent, oxyma-derived uronium salt (1-cyano-2-ethoxy-2- oxoethylidenaminooxy)dimethylamino-morpholino-carbenium hexafluorophosphate, COMU), which improves a coupling efficiency in aqueous media, was introduced to catalyze the formation of amide bonds.[51] First, PPDT-P/PSMA,PPDT-P/T-DCS/PSMA, and PPDT-P/ITIC/PSMA Pdots were concentrated via centrifugal filtration (100 μL, 0.35 mg/mL). Then, each concentrated Pdot solution was mixed with polyethylene glycol (5% PEG in deionized water, 4000 Da),[6] freshly prepared COMU (100 μL, 5.4 mM), *N*-methylmorpholine (NMM, 6 μL, 0.2 M) and the amine-containing secondary antibody to conjugate (30 μL, 1.3 mg/mL) in deionized water. The reaction mixture was stirred overnight at room temperature. After antibody conjugation, the remaining carboxylic acid groups were subsequently blocked with amine-containing oligoethylene glycol (OEG) chains to prevent the non-specific adsorption of Pdots during immunostaining (Figure S11). The purification of Pdot/antibody conjugates was optimized via a two-step procedure involving size-exclusion chromatography (SEC, Nap-5 columns packed with Sephadex G-25 DNA grade resin) and centrifugal filtration.[52-54] As shown in **Figure 5**a and c, the PPDT-P/PSMA/antibody conjugate exhibited slightly faster elution than the Pdot itself, owing to the increased size with antibody conjugation. Because the antibodies were colorless and non-fluorescent, they were reacted with commercially available Alexa Fluor 568 containing a *N*-hydroxysuccinimide (NHS) ester group, allowing their elution to be monitored. Because most of immunoglobulin G (IgG) antibodies show similar molecular weight (~150 kDa), Donkey anti-Rat secondary antibodies was chosen and tested for SEC purification.[55] According to the elution tests of unreacted secondary antibodies (Figure 5b), free antibodies appeared from 7th tube, which overlaps with the elution range of the Pdot/antibody conjugates (4th–9th tubes),

requiring a further purification to remove the excess free antibodies after coupling reaction. After SEC, the collected mixtures of the Pdot/antibody conjugates and free excess antibodies were separated via centrifugal filtration (molecular weight cutoff, 300K). The residue was re-dispersed into phosphate-buffered saline (PBS), and centrifugal filtration was repeated three times to ensure that no free antibodies remained (Figure 5d). After antibody conjugation, a broad absorption at ~280 nm appeared in the UV–vis absorption spectra, indicating the successful coupling of antibodies on the surface of the Pdots (Figure S12).

2.4. Single staining of Pdot/antibody conjugates

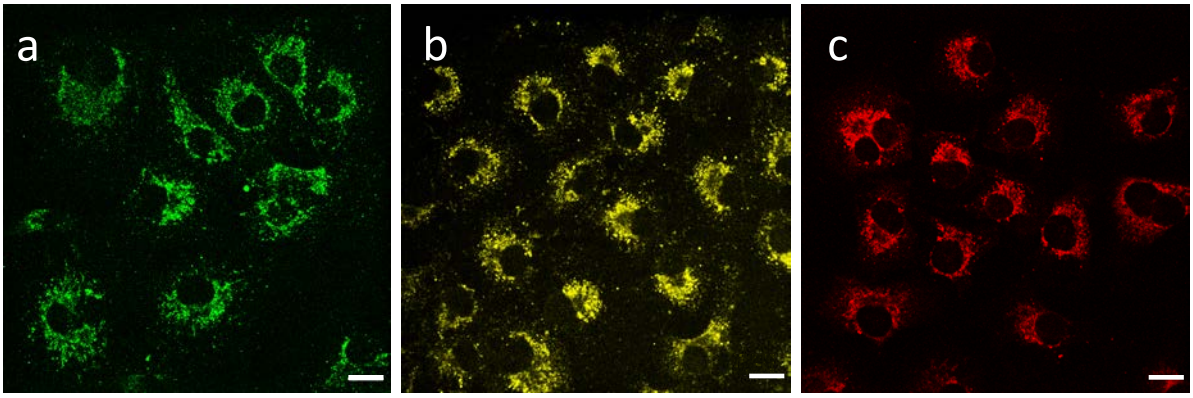

Figure 6. Confocal fluorescence images of mitochondria in COS-7 cells with three different emission colors. Fluorescence signals from (a) PPDT-P/PSMA, (b) PPDT-P/T-DCS/PSMA, and (c) PPDT-P/ITIC/PSMA Pdots with 525/50 nm, 600/50 nm, and 700/75 nm emission filters, respectively. All images were obtained by excitation with a 405 nm laser. The scale bars represent 20 μm.

Prior to the simultaneous immunostaining of all three Pdot/antibody conjugates, an independent staining test of each Pdot/antibody conjugate was performed to verify the specific binding to target organelles and spectral leakthroughs. By combining the green-, red-, and NIR-emitting Pdots with Donkey anti-Rabbit, we prepared three Pdot/antibody conjugates specific to mitochondria. Mitochondria labeling in COS-7 cells was performed with sequential incubation of the Rabbit anti-Tom20 primary antibody and three types of Pdot/anti-Rabbit conjugates. As shown in **Figure 6**, typical mitochondria images in three different emission colors were obtained, indicating the specific targeting of Pdot/antibody conjugates via the immunostaining process. Target specificity of Pdot/antibody conjugates was further investigated via colocalization analysis of the Pdot conjugates with a commercial mitochondria-targeting dye (Figure S13). The resultant two-color images of MitoTracker Deep Red and

PPDT-P/PSMA Pdots/Donkey anti-Rabbit IgG show colocalization of the two different probes on mitochondria. In contrast, unconjugated Pdots without antibodies yielded nonspecific staining of COS-7 cells, suggesting that the Pdots did not perturb the antibody specificity (Figure S14). All the FRET-based Pdots were suitable for excitation with the same wavelength because of their identical absorption at λ_{abs} = ~420 nm, which well matched a commercially available 405 nm laser source. Importantly, the FRET-based Pdots as a multicolor imaging platform with a single excitation source can be extended to cover more target structures by modifying the target-specific primary antibodies and paired secondary antibodies conjugated to the Pdot surface.

Before simultaneous immunostaining of COS-7 cells, the green-emissive PPDT-P/PSMA/anti-Rat, red-emissive PPDT-P/T-DCS/PSMA/anti-Mouse, and NIR-emissive PPDT-P/ITIC/PSMA/anti-Rabbit conjugates were first tested for specific targeting of tubulin, vimentin, and mitochondria, separately. While the excitation laser was fixed at 405 nm, the emissions of the three Pdots were distinguished using three emission bandpass filters. The green fluorescence image of tubulin was detected with a 525/50 nm emission filter, and no recognizable images were obtained with the 600/50 and 700/75 nm filters (Figure S15a–c). The vimentin and mitochondria images via the FRET-mediated red and NIR emissions were acquired with a 600/50 and 700/75 nm filter set, respectively and exhibited little spectral leakthrough. The residual fluorescence of the donor fluorophore was observed in the 525/50 nm emission channel, but it was 7-8% of the signal intensity in the acceptor channels for T-DCS and ITIC (Figure S15d and g). The color purities of the green-, red-, and NIR-emitting Pdots allowed fluorescence signals to be obtained only with the corresponding emission filter, enabling efficient separation of images of different targets with standard filter sets for constructing multicolor images.

In addition, the FRET-induced and directly excited confocal fluorescence images were compared by changing the excitation wavelengths (Figure S16). For cell images acquired by direct excitation of acceptors, the 561 nm and 637 nm lasers were utilized to excite T-DCS and ITIC moieties, respectively. In COS-7 cells stained with PPDT-P/T-DCS/PSMA/Donkey anti-Mouse IgG (vimentin) or PPDT-P/ITIC/PSMA/Donkey anti-Rabbit IgG (mitochondria), red-emissive vimentin or NIR-emissive mitochondria confocal microscopy images were obtained by exciting PPDT-P (at 405 nm) or acceptors (T-DCS and ITIC at 561 and 637 nm, respectively). As shown in Figure S16, the FRET-induced confocal images are much brighter (by 5-7 times) compared to those by directly exciting T-DCS and ITIC, emphasizing the advantages of FRET-based multicolor imaging.

2.5. Simultaneous multicolor imaging with a single wavelength excitation

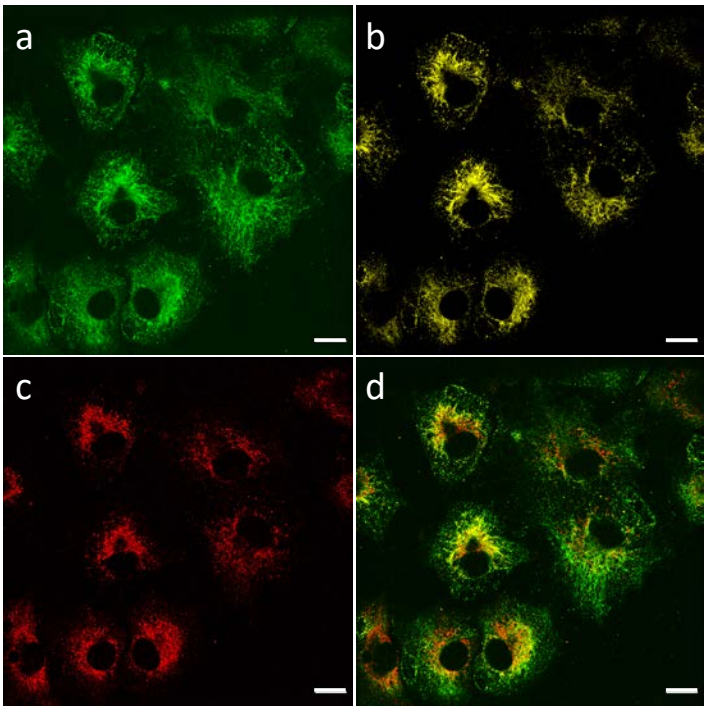

Figure 7. Three-color confocal microscopy images of COS-7 cells co-labeled with all three Pdot/antibody conjugates by switching the emission filters: (a) tubulin, (b) vimentin, and (c)

mitochondria. (d) Overlaid images of panels (a)–(c). All images were collected by excitation with a 405 nm laser. The scale bars are 20 μm.

Encouraged by the confocal images by separate staining of each type of Pdot, three Pdot/antibody probes specific for three types of targets were immunostained simultaneously in COS-7 cells (**Figure 7**). First, the mixture of primary antibodies of Rat anti-tubulin, Mouse anti-vimentin, and Rabbit anti-Tom20 (mitochondria) were incubated with COS-7 cells, allowing secondary antibody-coupled Pdots to target the specific subcellular organelles. All three types of Pdot/antibody conjugates were simultaneously incubated together because all the secondary antibodies labeled on the Pdot surfaces were chosen to have minimal cross-reactivity, except for their target antigen, and came from the same host species (Donkey). It was possible to achieve highly selective binding of the Pdot/antibody conjugates to the corresponding target even when different Pdot/antibody conjugates were mixed together without the need for tedious sequential immunostaining. As shown in Figure 7, multicolor images of the three subcellular structures from the Pdot/antibody conjugates were successfully obtained by excitation with a single laser (405 nm) and simply switching the emission filters for green-emissive tubulin, red fluorescing vimentin and NIR-emitting mitochondria.

3. CONCLUSION

We prepared FRET-based green-, red-, and NIR-emitting Pdots and employed them for multicolor cell imaging with a single excitation wavelength. The green-emissive conjugated polymer (PPDT-P) was precipitated alone or co-precipitated with a FRET acceptor (T-DCS or ITIC), facilitating FRET-mediated red and NIR emission. The FRET donor-acceptor pairs were carefully optimized to show the remarkably high FRET efficiency (80-98%) and FRET-mediated emissions with high color purity. The FRET-mediated red and NIR signals were amplified (via the antenna effect) by a factor of 5.3–8.5 relative to those obtained via the direct excitation of acceptors, emphasizing the advantages of FRET-based imaging. The covalent immobilization of target-specific antibodies onto the surface of Pdots yielded active targeting Pdot/antibody probes. Three Pdot/antibody probes specific for subcellular organelles (tubulin, vimentin, and mitochondria) were simultaneously co-stained in COS-7 cells, reducing the tedious sequential immunostaining process to a single step. Highly selective binding of the Pdot/antibody conjugates to the corresponding targets was observed even when different Pdot/antibody probes were mixed together. Thus, high-contrast three-colored cell images were obtained with a single excitation wavelength, by simply changing the emission filter. Our new strategy for simultaneous multicolor cellular imaging based on FRET-induced emission with a single excitation is a cost-effective and time-saving multicolor imaging technique for cell biological investigations. By simply changing the labeling antibodies, it is also possible to further extend the target molecules for multicolor imaging of other cellular structures.

4. EXPERIMENTAL SECTION

4.1. Chemicals

FRET acceptor, ITIC was purchased from Solarmer (Beijing, China). The amphiphilic functional polymer PSMA (average M_n ~1600 Da, ~1.3:1 mole ratio of styrene:maleic anhydride), COMU, and NMM were purchased from Sigma–Aldrich (St. Louis, MO, USA). PEG (MW = 4000 Da) was purchased from Tokyo Chemical Industry (TCI) Co., Ltd. (Tokyo, Japan). The primary antibodies, Rat anti-Tubulin (ab6160) and Rabbit anti-beta Tubulin (ab6046) were purchased from Abcam (Cambridge, UK). Rabbit anti-Tom20 (sc-11415) and Mouse anti-Vimentin (M0725) were purchased from Santa Cruz Biotechnology (Texas, USA), and Dako (Glostrup, Denmark), respectively. For surface modification for targeting, Donkey anti-Rat (712-005-153), Donkey anti-Mouse (715-005-151), and Donkey anti-Rabbit (711-005-152) secondary antibodies were purchased from Jackson Immuno Research Laboratories, Inc. (Pennsylvania, USA). MitoTracker Deep Red was purchased from Thermo Fisher Scientific (Massachusetts, USA). All chemicals and biomolecules were used as received, unless otherwise specified. NAP-5 gel columns were purchased from GE Healthcare (Chicago, USA).

4.2. Synthesis of PPDT-P and T-DCS

Synthesis of Intermediates

M1 and compound 6 were prepared via previously reported procedures.[23, 24] To prepare M2, a mixture of 2,5-dibromoterephthalic acid (2.5 g, 7.7 mmol) and $SOCl_2$ (30 mL) was heated under reflux overnight. The solution was cooled, and the excess $SOCl_2$ was evaporated, to which a solution comprising of 2-hexyl-1-decanol (6.4 g, 26.5 mmol) in pyridine (20 mL) was added dropwise. The mixture was heated at 80 ℃ for 18 h and then cooled to room temperature. The reaction mixture was poured into a cold 1 M HCl, and the product was extracted with ethyl

acetate (EA). The organic layer was then washed with saturated $NaHCO_3$ and brine, and the solvent was evaporated. The product was purified via silica gel chromatography using EA/hexane (1:4, by volume) as the eluent, yielding colorless oil. Yield: 70%. ^{1}H NMR (500 MHz, $CDCl_3$): δ (ppm) 7.99 (s, 2H), 4.25 (m, 4H), 1.75 (m, 2H), 1.28 (m, 48H), 0.86 (m, 12H). ^{13}C NMR (125 MHz, $CDCl_3$): δ (ppm) 164.62, 136.55, 136.01, 120.03, 69.22, 37.40, 31.97, 31.88, 31.37, 30.0, 29.67, 29.63, 29.38, 26.78, 26.76, 22.76, 22.73, 14.20, 14.18.

Synthesis of PPDT-P

M1 (121 mg, 0.21 mmol) and M2 (165 mg, 0.21 mmol) were added to a 2 mL microwave vial. $Pd_2(dba)_3$ (2 mol%) as a catalyst and tri(*o*-tolyl)phosphine (8 mol%) as a ligand were added to the above reaction mixture in a glovebox. After the microwave vial was capped, anhydrous toluene (1.5 mL) was added using a syringe. Polymerization was conducted in a microwave reactor at 140 °C for 60 min. The resulting polymer was precipitated into methanol, and the precipitate was subjected to Soxhlet extraction with methanol, hexane, and chloroform. The extracted polymer in chloroform was precipitated into methanol and dried under vacuum, yielding a final polymer of PPDT-P. Yield: 78%. M_n = 22,600 Da and polydispersity index (PDI) = 1.8. ^{1}H NMR (500 MHz, $CDCl_3$): δ (ppm) 7.86 (Br, 2H), 7.63 (Br, 4H), 7.32 (Br, 2H), 7.10 (Br, 2H), 4.13 (Br, 4H), 1.55 (m, 2H), 1.18 (m, 48H), 0.83 (m, 12H). ^{13}C NMR (125 MHz, $CDCl_3$): δ (ppm) 167.82, 144.64, 139.61, 133.49, 132.89, 132.52, 131.25, 127.56, 125.63, 123.19, 68.37, 36.79, 31.47, 31.43, 30.63, 29.51, 29.16, 28.90, 26.34, 26.31, 22.26, 22.22, 13.70, 13.68.

Synthesis of T-DCS

To prepare T-DCS, a 25 mL two-neck round-bottom flask was filled with compound 6 (0.2 g, 0.203 mmol), 2-(tributylstannyl)thiophene (0.19 g, 0.509 mmol), $Pd_2(dba)_3$ (4 mol%), and tri(*o*-tolyl)phosphine (8 mol%). Under nitrogen, anhydrous toluene (10 mL) was added,

followed by refluxing at 120 ℃ overnight for a Stille coupling reaction. After the reaction was completed, the reaction mixture was extracted using chloroform and water. The organic layer was dried over anhydrous $MgSO_4$, and the solvent was removed via rotary evaporation. The reaction mixture was purified via column chromatography (1:1 chloroform/hexane by volume as an eluent) and recrystallization using methanol. Yield: 72%. ^{1}H NMR (500 MHz, $CDCl_3$): δ (ppm) 7.88 (s, 2H), 7.86 (s, 2H), 7.33 (d, 2H), 7.31 (d, 2H), 7.25 (d, 2H), 7.31 (d, 2H), 7.08 (dd, 2H), 4.04 (d, 4H), 1.94-1.87 (m, 2H), 1.56-1.20 (m, 48H), 0.87 (t, 12H). ^{13}C NMR (125 MHz, $CDCl_3$): δ (ppm) 151.73, 138.63, 138.52, 136.55, 132.44, 128.09, 128.04, 125.57, 125.47, 124.56, 124.37, 116.94, 110.63, 105.75, 72.20, 38.17, 31.92, 31.89, 31.74, 31.73, 30.16, 29.82, 29.65, 29.40, 27.04, 27.01, 22.71, 14.12, 14.11. MALDI-TOF ($C_{60}H_{80}N_2O_2S_4$): 988.4862.

4.3. Preparation of Pdots

Pdots were prepared via a nanoprecipitation method, by modification of previous reports.[7, 8, 25] The stock solutions (1 mg/mL) of FRET donor polymer (PPDT-P), two types of FRET acceptors (T-DCS and ITIC) and PSMA were prepared in THF. For green-emissive Pdots, the PPDT-P (100 μL) and PSMA (400 μL) stock solutions were added into 4.5 mL THF to yield a solution of [PPDT-P] = 20 μg/mL. A series of red- and NIR-emissive Pdots was prepared by varying the mixing ratio of donor and acceptor stock solutions, e.g., 80:20 μL, 60:40 μL, 40:60 μL, and 20:80 μL, to form fluorophore solutions with a total volume of 100 μL. Then, fluorophore solutions for red- and NIR-emissive Pdots ([PPDT-P] = 4–18 μg/mL and [T-DCS or ITIC] = 2–16 μg/mL) were added to a mixture of PSMA stock solution (400 μL) and THF (4.5 mL). After vigorous sonication, 5 mL of the precursor solution was quickly transferred to 10 mL of deionized water in a bath sonicator. The solution was concentrated to 2 mL via continuous evaporation under a stream of nitrogen gas in a 90 ℃ bath, producing a Pdot solution

with a 50 μg/mL concentration of emitting species. The concentrated Pdot solution was filtered through a 0.1 μm syringe filter and kept in a brown-colored vial.

4.4. Conjugation of secondary antibody and Pdots

Conjugation between the carboxylic acid groups on the Pdot surfaces and amine-containing secondary antibodies was performed by utilizing the COMU-catalyzed reaction in the presence of NMM as a base. The Pdot solution (700 μL, 50 μg/mL) prepared as described above was concentrated by utilizing Nanosep Omega 10K centrifugal devices. The concentrated green, red, or NIR Pdot solution (100 μL, 350 μg/mL) and 10 μL of PEG (5% in deionized water, 4000 Da) were transferred to a clean reaction tube with a Teflon-coated stir bar. After the reaction mixture of Pdot and 6 μL of 0.2 M NMM was stirred for 5 min, 100 μL of freshly prepared COMU in deionized water (5.4 mM) was added. 30 μL of three types of amine-containing secondary antibodies (1.3 mg/mL each) were added to the corresponding Pdot solutions. The resulting mixtures were continuously stirred via magnetic stirring overnight at room temperature. Lastly, a solution comprising 3-(2-(2-methoxyethoxy)ethoxy)-2-((2-(2-methoxyetoxy)ethoxy)methyl)propan-1-amine in water (15 μL, 2 mg/mL) was added, followed by stirring for an additional 3 h. The reaction mixture was purified via the following procedures.

4.5. Purification of Pdot/antibody conjugates

The reaction mixture was first purified via gel column chromatography and centrifugal filtration was also performed to remove the unreacted excess antibodies. Because Nap-5 columns are packed with Sephadex G-25 DNA-grade resin, the size exclusion chromatography (SEC) column separates materials according to their size. After a gel column was equilibrated by running three column volumes of PBS, the sample solution (~260 μL) was loaded to the

center of the column and was allowed to enter into the column. Owing to their strong emission, the Pdots and Pdot/antibody conjugates could be easily collected by receiving the drops by monitoring their elution with a handheld UV lamp (365 nm). The Pdot/antibody conjugates were first separated by collecting the 7^{th}–18^{th} eluent drops after the sample was loaded. Then, the eluted solution was filtrated using a Nanosep Omega 300K centrifugal device for 5 min at 5000 rpm. The filtered part was re-dispersed in PBS, and centrifugal filtration was repeated two more times to ensure that no free antibodies remained. The purified Pdot/antibody conjugates were stored in a refrigerator (4 ℃) before use.

4.6. Cell culture and immunostaining

COS-7 cells (Korean Collection for Type Cultures, KCTC) were cultured in DMEM (SH30022.01, Hyclone) with 10% fetal bovine serum (FBS, 97068-085, VWR Life Science) and 1% antibiotics-antimycotics (15240-062, Gibco). All cells were grown in an incubator at 37 ℃ in 5% CO_2. The COS-7 cells were grown on coverslip-bottomed 8-well chambers (155409, LAB-TEK) overnight. After fixation with 4% paraformaldehyde (PFA, 50-980-495, Electron Microscopy Science) for 15 min, the samples were washed with PBS three times, followed by reduction in 10 mM $NaBH_4$ (71320, Sigma Aldrich) for 5 min. After rinsing, the samples were permeabilized with 0.5% Triton X-100 in PBS for 5 min and blocked with 3% BSA with 0.5% Triton X-100 in PBS for 30 min. Then, the samples were incubated with diluted primary antibodies in blocking buffer (3% BSA + 0.5% Triton X-100 in PBS)—Rat anti-Tubulin (2 μg/mL, 1:500 dilution), Rabbit anti-Tom20 (4 μg/mL, 1:50 dilution), and Mouse anti-Vimentin (4 μg/mL, 1:50 dilution)—for 1 h. After being washed with a washing buffer (0.1% Triton X-100 in PBS) three times, the samples were incubated with secondary antibody-labeled Pdots in a blocking buffer for 2 h. The resulting samples were washed three times with

the washing buffer and post-fixed for 5 min with 4% PFA, followed by washing three times with PBS. All immunostaining steps were performed at room temperature. For co-immunostaining of three types of probes, the fixed and blocked cells were incubated with the mixture of all primary antibodies first and then incubated in the mixture of three secondary antibody/Pdot conjugates. Because there was no obvious crosstalk between the different Pdot/antibody conjugates, the tedious immunostaining was reduced to a single step, avoiding the repeated incubation and washing steps.

4.7. Confocal image acquisition

Confocal fluorescence images were obtained with a spinning-disk confocal microscope (DragonFly, Andor) with a 60×/1.2 NA water Nikon objective. Three types of Pdots were excited with a 405 nm direct diode laser (Solid state 405 smart diode laser, 100 mW), and the emissions were distinguished by 525/50 nm, 600/-50 nm and 700/-75 nm emission filters for green-, red-, and NIR-emitting Pdots, respectively. For comparison of FRET-induced and directly excited fluorescence images, the 561 nm (Solid state 560 OPSL smart laser, 150 mW) and 637 nm diode lasers (OBIS LX Solid state 637 smart diode laser, 140 mW) were utilized to excite T-DCS and ITIC, respectively. The emission filters were mounted in a motorized filter wheel and controlled by the acquisition software. The images were analyzed using a commercial software, Imaris (Oxford Instruments) and an open-source software, ImageJ.

Acknowledgements

This work was supported by the Korea University Grant and the National Research Foundation (NRF) of Korea (2019R1A2C2085290, 2017K2A9A2A12000315, 2019R1A6A1A11044070). This work was supported by IBS-R023-D1 for H.-C.K., M.K. and S.-H.S. M.A.U. acknowledges the Juan De La Cierva postdoctoral fellowship.

Supporting Information.

The Supporting Information is available free of charge on the ACS Publication website at DOI: Synthesis of PPDT-P and T-DCS, preparation and characterization of Pdots and Pdot/antibody conjugates, cell culture, immunostaining and confocal image acquisition.

References

1. McQuade, D. T.; Pullen, A. E.; Swager, T. M., Conjugated polymer-based chemical sensors. *Chem. Rev.* **2000,** 100, 2537-2574.
2. Thomas, S. W. III.; Joly, G. D.; Swager, T. M., Chemical sensors based on amplifying fluorescent conjugated polymers. *Chem. Rev.* **2007,** 107, 1339-1386.
3. Pu, K. Y.; Liu, B., Fluorescent Conjugated Polyelectrolytes for Bioimaging. *Adv. Funct. Mater.* **2011,** 21, 3408-3423.
4. Jeong, J. E.; Woo, S. J.; Le, V. S.; Choi, H.; Woo, H. Y., Combination of conjugated polyelectrolytes and biomolecules: A new optical platform for highly sensitive and selective chemo- and biosensors. *Macromol Res* **2014,** 22, 461-473.
5. Zhou, Q.; Swager, T. M., Methodology for enhancing the sensitivity of fluorescent chemosensors: energy migration in conjugated polymers. *J. Am. Chem. Soc.* **1995,** 117, 7017-7018.
6. Wu, C. F.; Hansen, S. J.; Hou, Q. O.; Yu, J. B.; Zeigler, M.; Jin, Y. H.; Burnham, D. R.; McNeill, J. D.; Olson, J. M.; Chiu, D. T., Design of Highly Emissive Polymer Dot Bioconjugates for In Vivo Tumor Targeting. *Angew. Chem. Int. Ed.* **2011,** 50, 3430-3434.
7. Wu, C. F.; Schneider, T.; Zeigler, M.; Yu, J. B.; Schiro, P. G.; Burnham, D. R.; McNeill, J. D.; Chiu, D. T., Bioconjugation of Ultrabright Semiconducting Polymer Dots for Specific Cellular Targeting. *J. Am. Chem. Soc.* **2010,** 132, 15410-15417.
8. Wu, C. F.; Chiu, D. T., Highly Fluorescent Semiconducting Polymer Dots for Biology and Medicine. *Angew. Chem. Int. Ed.* **2013,** 52, 3086-3109.

9. Chinen, A. B.; Guan, C. M.; Ferrer, J. R.; Barnaby, S. N.; Merkel, T. J.; Mirkin, C. A., Nanoparticle Probes for the Detection of Cancer Biomarkers, Cells, and Tissues by Fluorescence. *Chem. Rev.* **2015,** 115, 10530-10574.
10. Wang, H.; Zhang, P. S.; Hong, Y. X.; Zhao, B.; Yi, P. G.; Chen, J., Ratiometric imaging of lysosomal hypochlorous acid enabled by FRET-based polymer dots. *Polymer Chemistry* **2017,** 8, 5795-5802.
11. Ye, F. M.; Wu, C. F.; Jin, Y. H.; Wang, M.; Chan, Y. H.; Yu, J. B.; Sun, W.; Hayden, S.; Chiu, D. T., A compact and highly fluorescent orange-emitting polymer dot for specific subcellular imaging. *Chem. Commun.* **2012,** 48, 1778-1780.
12. Wang, Z. Y.; Wang, C.; Fang, Y. Y.; Yuan, H.; Quan, Y. W.; Cheng, Y. X., Color-tunable AIE-active conjugated polymer nanoparticles as drug carriers for self-indicating cancer therapy via intramolecular FRET mechanism. *Polym. Chem.* **2018,** 9, 3205-3214.
13. Kim, C.; Kim, S. Y.; Lim, Y. T.; Lee, T. S., Synthesis of conjugated polymer nanoparticles with core-shell structure for cell imaging and photodynamic cancer therapy. *Macromol Res* **2017,** 25, 572-577.
14. Rong, Y.; Wu, C. F.; Yu, J. B.; Zhang, X. J.; Ye, F. M.; Zeigler, M.; Gallina, M. E.; Wu, I. C.; Zhang, Y.; Chan, Y. H.; Sun, W.; Uvdal, K.; Chiu, D. T., Multicolor Fluorescent Semiconducting Polymer Dots with Narrow Emissions and High Brightness. *ACS Nano* **2013,** 7, 376-384.
15. Garbacik, E. T.; Sanz-Paz, M.; Borgman, K. J. E.; Campelo, F.; Garcia-Parajo, M. F., Frequency-Encoded Multicolor Fluorescence Imaging with Single-Photon-Counting Color-Blind Detection. *Biophys. J.* **2018,** 115, 725-736.
16. Fang, C. C.; Chou, C. C.; Yang, Y. Q.; Wei-Kai, T.; Wang, Y. T.; Chan, Y. H., Multiplexed Detection of Tumor Markers with Multicolor Polymer Dot-Based Immunochromatography Test Strip. *Anal. Chem.* **2018,** 90, 2134-2140.
17. Wu, C.; Bull, B.; Szymanski, C.; Christensen, K.; McNeill, J., Multicolor Conjugated Polymer Dots for Biological Fluorescence Imaging. *ACS Nano* **2008,** 2, 2415-2423.
18. Cheng, C. G.; Xing, M.; Wu, Q. L., Preparation of carbon dots with long-wavelength and photoluminescence-tunable emission to achieve multicolor imaging in cells. *Opt. Mater.* **2019,** 88, 353-358.
19. Hu, F.; Cai, X. L.; Manghnani, P. N.; Kenry; Wu, W. B.; Liu, B., Multicolor monitoring of cellular organelles by single wavelength excitation to visualize the mitophagy process. *Chem. Sci.* **2018,** 9, 2756-2761.
20. Lakowicz, J. R., *Principles of Fluorescence Spectroscopy*. 3rd ed.; Springer US: 2006.
21. Jeong, J.-E.; Kim, B.; Woo, S.; Hwang, S.; Bazan, G. C.; Woo, H. Y., Principal factors that determine the extension of detection range in molecular beacon aptamer/conjugated polyelectrolyte bioassays. *Chem. Sci.* **2015,** 6, 1887-1894.
22. Liu, B.; Gaylord, B. S.; Wang, S.; Bazan, G. C., Effect of chromophore-charge distance on the energy transfer properties of water-soluble conjugated oligomers. *J. Am. Chem. Soc.* **2003,** 125, 6705-6714.
23. Ko, S. J.; Hoang, Q. V.; Song, C. E.; Uddin, M. A.; Lim, E.; Park, S. Y.; Lee, B. H.; Song, S.; Moon, S. J.; Hwang, S.; Morin, P. O.; Leclerc, M.; Su, G. M.; Chabinyc, M. L.; Woo,

H. Y.; Shin, W. S.; Kim, J. Y., High-efficiency photovoltaic cells with wide optical band gap polymers based on fluorinated phenylene-alkoxybenzothiadiazole. *Energy Environ. Sci.* **2017,** 10, 1443-1455.

24. Ryu, H. S.; Kim, M. J.; Kang, M. S.; Cho, J. H.; Woo, H. Y., Dicyanodistyrylbenzene-Based Copolymers for Ambipolar Organic Field-Effect Transistors with Well-Balanced Hole and Electron Mobilities. *Macromolecules* **2018,** 51, 8258-8267.
25. Wu, C. F.; Jin, Y. H.; Schneider, T.; Burnham, D. R.; Smith, P. B.; Chiu, D. T., Ultrabright and Bioorthogonal Labeling of Cellular Targets Using Semiconducting Polymer Dots and Click Chemistry. *Angew. Chem. Int. Ed.* **2010,** 49, 9436-9440.
26. Koskikallio, J., Kinetics of the Hydrolysis and Formation of Dimethylmaleic Anhydride in Solvent Mixtures. *Acta Chem. Scand.* **1956,** 10, 822-830.
27. Yu, J.; Wu, C.; Zhang, X.; Ye, F.; Gallina, M. E.; Rong, Y.; Wu, I.-C.; Sun, W.; Chan, Y.-H.; Chiu, D. T., Stable Functionalization of Small Semiconducting Polymer Dots via Covalent Cross-Linking and Their Application for Specific Cellular Imaging. *Adv. Mater.* **2012**, 24, 3498-3504.
28. Mei, J. G.; Bao, Z. N., Side Chain Engineering in Solution-Processable Conjugated Polymers. *Chem. Mater.* **2014,** 26, 604-615.
29. Twomey, M.; Vokata, T.; Kumar, M. R.; Moon, J. H., Differential interactions of conjugated polymer nanoparticles with glycosaminoglycans in synthetic urine. *Chem. Commun.* **2015,** 51, 4065-4068.
30. Vokata, T.; Twomey, M.; Mendez, E.; Moon, J. H., Synthesis of Biodegradable Conjugated Polymers with Controlled Backbone Flexibility. *J. Polym. Sci. Pol. Chem.* **2015,** 53, 1403-1412.
31. Zgou, H.; Bouzzine, S. M.; Bouzakraoui, S.; Hamidi, M.; Bouachrine, M., Theoretical study of structural and electronic properties of oligo(thiophene-phenylene)s in comparison with oligothiophenes and oligophenylenes. *Chin. Chem. Lett.* **2008,** 19, 123-126.
32. Zgou, H.; Hamidi, M.; Bouachrine, M., DFT calculations of the local spin densities and oligomerization mechanism of thiophene-phenylene (TP) co-oligomers and derivatives. *J Mol Struc-Theochem* **2007,** 814, 25-32.
33. Swager, T. M., The molecular wire approach to sensory signal amplification. *Acc. Chem. Res.* **1998,** 31, 201-207.
34. Liu, B.; Bazan, G. C., Optimization of the molecular orbital energies of conjugated polymers for optical amplification of fluorescent sensors. *J. Am. Chem. Soc.* **2006,** 128, 1188-1196.
35. Jin, Y. H.; Ye, F. M.; Zeigler, M.; Wu, C. F.; Chiu, D. T., Near-Infrared Fluorescent Dye-Doped Semiconducting Polymer Dots. *ACS Nano* **2011,** 5, 1468-1475.
36. Sun, K.; Chen, H. B.; Wang, L.; Yin, S. Y.; Wang, H. Y.; Xu, G. X.; Chen, D. N.; Zhang, X. J.; Wu, C. F.; Qin, W. P., Size-Dependent Property and Cell Labeling of Semiconducting Polymer Dots. *ACS Appl. Mater. Interfaces* **2014,** 6, 10802-10812.

37. Wu, C. F.; Zheng, Y. L.; Szymanski, C.; McNeill, J., Energy transfer in a nanoscale multichromophoric system: Fluorescent dye-doped conjugated polymer nanoparticles. *J. Phys. Chem. C* **2008,** 112, 1772-1781.
38. Fung, B. K. K.; Stryer, L., Surface Density Determination in Membranes by Fluorescence Energy-Transfer. *Biochemistry* **1978,** 17, 5241-5248.
39. Antony, T.; Saxena, A.; Roy, K. B.; Bohidar, H. B., Laser light scattering immunoassay: An improved data analysis by CONTIN method. *J Biochem Bioph Meth* **1998,** 36, 75-85.
40. Clafton, S. N.; Beattie, D. A.; Mierczynska-Vasilev, A.; Acres, R. G.; Morgan, A. C.; Kee, T. W., Chemical Defects in the Highly Fluorescent Conjugated Polymer Dots. *Langmuir* **2010,** 26, 17785-17789.
41. Rohatgi, C. V.; Harada, T.; Need, E. F.; Krasowska, M.; Beattie, D. A.; Dickenson, G. D.; Smith, T. A.; Kee, T. W., Low-Bandgap Conjugated Polymer Dots for Near-Infrared Fluorescence Imaging. *Acs Appl Nano Mater* **2018,** 1, 4801-4808.
42. Hanaor, D.; Michelazzi, M.; Leonelli, C.; Sorrell, C. C., The effects of carboxylic acids on the aqueous dispersion and electrophoretic deposition of ZrO2. *J. Eur. Ceram. Soc.* **2012,** 32, 235-244.
43. Zhang, D.; Wu, M.; Zeng, Y. Y.; Liao, N. S.; Cai, Z. X.; Liu, G.; Liu, X. L.; Liu, J. F., Lipid micelles packaged with semiconducting polymer dots as simultaneous MRI/photoacoustic imaging and photodynamic/photothermal dual-modal therapeutic agents for liver cancer. *J Mater Chem B* **2016,** 4, 589-599.
44. Ke, C. S.; Fang, C. C.; Yan, J. Y.; Tseng, P. J.; Pyle, J. R.; Chen, C. P.; Lin, S. Y.; Chen, J. X.; Zhang, X. J.; Chan, Y. H., Molecular Engineering and Design of Semiconducting Polymer Dots with Narrow-Band, Near-Infrared Emission for in Vivo Biological Imaging. *ACS Nano* **2017,** 11, 3166-3177.
45. Chen, C. P.; Huang, Y. C.; Liou, S. Y.; Wu, P. J.; Kuo, S. Y.; Chan, Y. H., Near-Infrared Fluorescent Semiconducting Polymer Dots with High Brightness and Pronounced Effect of Positioning Alkyl Chains on the Comonomers. *ACS Appl. Mater. Interfaces* **2014,** 6, 21585-21595.
46. Liu, Z. Y.; Chen, N.; Dong, C. H.; Li, W.; Guo, W. S.; Wang, H. J.; Wang, S.; Tan, J.; Tu, Y.; Chang, J., Facile Construction of Near Infrared Fluorescence Nanoprobe with Amphiphilic Protein-Polymer Bioconjugate for Targeted Cell Imaging. *ACS Appl. Mater. Interfaces* **2015,** 7, 18997-19005.
47. Pu, K. Y.; Li, K.; Shi, J. B.; Liu, B., Fluorescent Single-Molecular Core-Shell Nanospheres of Hyperbranched Conjugated Polyelectrolyte for Live-Cell Imaging. *Chem. Mater.* **2009,** 21, 3816-3822.
48. Wu, C. F.; Szymanski, C.; McNeill, J., Preparation and encapsulation of highly fluorescent conjugated polymer nanoparticles. *Langmuir* **2006,** 22, 2956-2960.
49. Lv, Y. L.; Liu, P.; Ding, H.; Wu, Y. S.; Yan, Y. L.; Liu, H.; Wang, X. F.; Huang, F.; Zhao, Y. S.; Tian, Z. Y., Conjugated Polymer-Based Hybrid Nanoparticles with Two-Photon Excitation and Near-Infrared Emission Features for Fluorescence Bioimaging within the Biological Window. *ACS Appl. Mater. Interfaces* **2015,** 7, 20640-20648.

50. Wang, S. W.; Liu, J.; Feng, G. X.; Ng, L. G.; Liu, B., NIR-II Excitable Conjugated Polymer Dots with Bright NIR-I Emission for Deep In Vivo Two-Photon Brain Imaging Through Intact Skull. *Adv. Funct. Mater.* **2019,** 29, 1808365.
51. Gabriel, C. M.; Keener, M.; Gallou, F.; Lipshutz, B. H., Amide and Peptide Bond Formation in Water at Room Temperature. *Org. Lett.* **2015,** 17, 3968-3971.
52. Chen, D. D.; Yuan, Y.; Yu, J. B.; Chiu, D. T.; Wu, C. F., Purification of Semiconducting Polymer Dots by Size Exclusion Chromatography Prior to Cytotoxicity Assay and Stem Cell Labeling. *Anal. Chem.* **2018,** 90, 5569-5575.
53. Hinterberger, V.; Damm, C.; Haines, P.; Guldi, D. M.; Peukert, W., Purification and structural elucidation of carbon dots by column chromatography. *Nanoscale* **2019,** 11, 8464-8474.
54. Trathnigg, B., Determination of Mwd and Chemical-Composition of Polymers by Chromatographic Techniques. *Prog. Polym. Sci.* **1995,** 20, 615-650.
55. Wang, W.; Singh, S.; Zeng, D. L.; King, K.; Nema, S., Antibody structure, instability, and formulation. *J. Pharm. Sci.* **2007,** 96, 1-26.

for Table of Contents use only

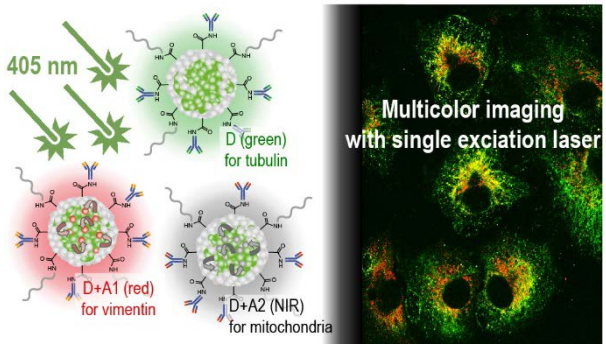

Green-, Red-, and NIR-Emitting Polymer Dot Probes for Simultaneous Multicolor Cell Imaging with a Single Excitation Wavelength

Ji-Eun Jeong,[†] Mohammad Afsar Uddin,[‡] Hwa Sook Ryu,[†] Hee-Chang Kim,[†,§] Minsu Kang,[†,§] Joonyoung Francis Joung,[†] Sungnam Park,[†] Sang-Hee Shim,[†,§,] and Han Young Woo[†,*]*